Crossover behavior of the thermal conductance and Kramers' transition rate theory

Kirill A. Velizhanin,[1,*] Subin Sahu,[2,3,4] Chih-Chun Chien,[5] Yonatan Dubi,[6] and Michael Zwolak[2,4,†]

[1] *Theoretical Division, Los Alamos National Laboratory, Los Alamos, NM 87545, USA*
[2] *Center for Nanoscale Science and Technology, National Institute of Standards and Technology, Gaithersburg, MD 20899, USA*
[3] *Maryland Nanocenter, University of Maryland, Collage Park, MD 20742, USA*
[4] *Department of Physics, Oregon State University, Corvallis, OR 97331, USA*
[5] *School of Natural Sciences, University of California, Merced, CA 95343, USA*
[6] *Department of Chemistry and the Ilse Katz Institute for Nanoscale Science and Technology, Ben-Gurion University of the Negev, Beer-Sheva 84105, Israel*

Kramers' theory frames chemical reaction rates in solution as reactants overcoming a barrier in the presence of friction and noise. For weak coupling to the solution, the reaction rate is limited by the rate at which the solution can restore equilibrium after a subset of reactants have surmounted the barrier to become products. For strong coupling, there are always sufficiently energetic reactants. However, the solution returns many of the intermediate states back to the reactants before the product fully forms. Here, we demonstrate that the thermal conductance displays an analogous physical response to the friction and noise that drive the heat current through a material or structure. A crossover behavior emerges where the thermal reservoirs dominate the conductance at the extremes and only in the intermediate region are the intrinsic properties of the lattice manifest. Not only does this shed new light on Kramers' classic turnover problem, this result is significant for the design of devices for thermal management and other applications, as well as the proper simulation of transport at the nanoscale.

Thermal transport is an important process in micro- and nano-scale technologies. It is often in a precarious position: On the one hand, thermal management strategies, including the engineering of low-resistance interfaces, become increasingly important as elements in electronic devices approach the atomic level. On the other hand, *phononics* – phonon analogues of electronics – seek tunability and inherently nonlinear behavior to make functional devices [1]. Thermal transport is thus at the forefront of nanotechnology research. Its impact in a broad array of applications has sparked advanced methods of the fabrication, control, and measurement of transport in, e.g., carbon nanotubes and single-molecule junctions [1–3].

Moreover, thermal transport is at the center of one of the major unresolved puzzles in theoretical physics, the absence of a derivation of Fourier's law of heat conduction from a microscopic Hamiltonian [4–9]. This is related to the seminal work of Fermi, Pasta and Ulam (FPU) [10–12], which demonstrated that nonlinearity does not always lead to thermalization. The considerations of FPU also apply to the emergence of a well-defined thermal conductivity. The role of nonlinearity – in addition to the description of the thermal reservoirs and interfacial regions – is thus the central topic of many studies examining thermal transport (see Refs. [5, 13, 14] for recent reviews).

In this work, we demonstrate that thermal transport goes through three physically distinct regimes as the coupling to the surrounding environment – the reservoir that supplies the heat – changes. For weak coupling, energy input from the reservoir limits the heat current through the entire system. For strong coupling, the lattice dynamics are distorted by the presence of the reservoir and this dominates the conductance. Thermal transport is determined by the intrinsic parameters of the

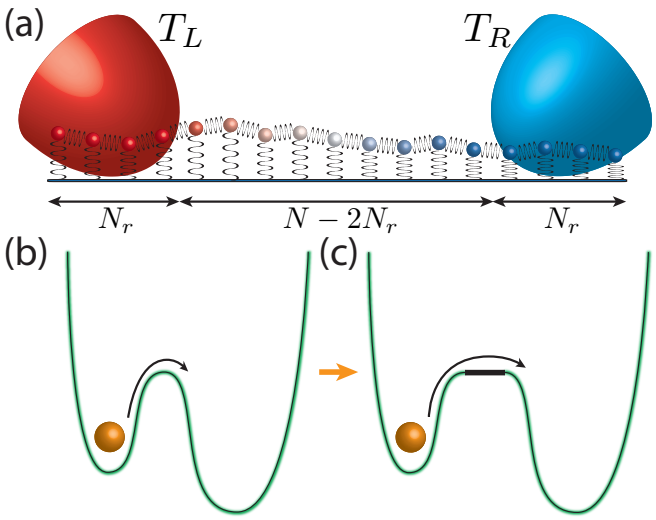

FIG. 1. Thermal conductance and Kramers' transition rate problem. (a) Schematic representation of a one-dimensional lattice of length N, with N_r sites on each side connected to independent Langevin reservoirs at temperatures T_L and T_R. (b) Kramers' problem where noise assists the escape of a classical particle from a metastable state. The green contour of the double-well potential outlines the region where the classical particle is subject to Langevin dynamics. (c) A modified double-well potential where the barrier is deformed horizontally into a region (thick black line) where only ballistic dynamics occurs, i.e., no friction or noise.

* kirill@lanl.gov
† mpz@nist.gov

lattice only in the intermediate regime. These three distinct regimes exist regardless of whether the system has a well-defined conductivity or not, as we will show by theoretically studying paradigmatic examples of thermal transport [5, 13, 15–17]. The dependence of the thermal conductance on the coupling strength to the reservoirs is physically analogous to the friction-induced turnover in Kramers' reaction rate problem for chemical reactions in solution.

RESULTS

The first model we examine is a classical one-dimensional (1D) uniform lattice of N harmonic oscillators. The Hamiltonian is

$$H = \frac{1}{2}\sum_{n=1}^{N} m\dot{x}_n^2 + \frac{D}{2}\sum_{n=1}^{N} x_n^2 + \frac{K}{2}\sum_{n=0}^{N}(x_n - x_{n+1})^2, \quad (1)$$

where x_n is the coordinate of the n^{th} oscillator, m is the mass, D is the strength of the on-site potential, and K is the nearest-neighbor coupling constant. The entire lattice is split into three regions: $N_r \geq 1$ sites on the left end (L) and on the right end (R) serve as *extended reservoirs* as each site (i.e., oscillator) in these regions is coupled to its own "external" Langevin reservoir of temperature T_L and T_R , see Fig. 1(a). The friction coefficient γ gives the strength of the coupling to the external reservoirs and is taken to be the same on the both ends for simplicity. The remaining $N - 2N_r$ sites in the middle comprise the *free lattice* (F). This is a generalization of a widely used model that sets $N_r \equiv 1$ [13, 15, 18]. In addition to being a prototypical model of thermal transport, it is also relevant to realistic systems, such as the high- and low-temperature limits of coarse-grained models of DNA [19, 20], where the on-site potential term represents the binding of interstrand base pairs.

Figure 2 shows the thermal conductance, defined as the heat current divided by $\Delta T = T_L - T_R$, for a long harmonic lattice with $N_r = 100$. A detailed description of the calculation is given in the supplementary information. Three qualitatively distinct regimes, which are labeled (1), (2) and (3), are apparent in the figure. We start by examining regime (2), where the conductance depends on γ only very weakly. The magnitude of the conductance on this plateau coincides with the *intrinsic conductance* of the lattice. For the anharmonic lattice we consider later on, the intrinsic conductance behaves as $\sim 1/N$ at large N, so there is a well-defined intrinsic *conductivity* in this plateau region, defined as the conductance multiplied by N in the limit $N \to \infty$.

Intrinsic conductance. We find the *intrinsic conductance* of the harmonic lattice by solving an auxiliary problem of the heat current between two semi-infinite ballistic (i.e., no friction) lattices. These lattices are initially disconnected and equilibrated at respective temperatures T_L and T_R. When connected, the heat current

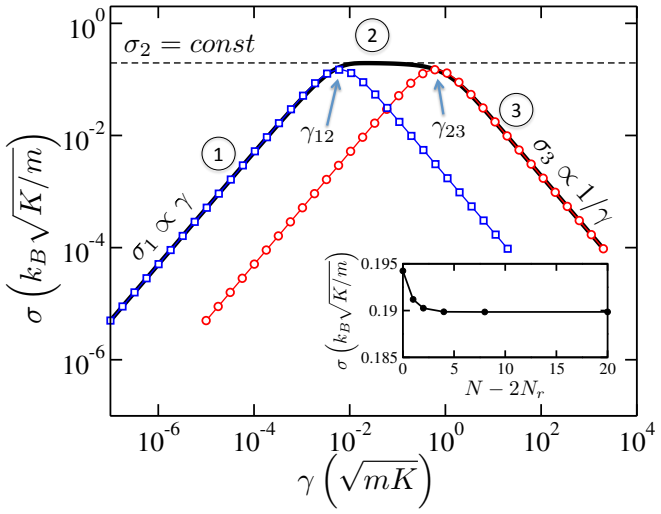

FIG. 2. The thermal conductance of a harmonic lattice with $D/K = 1$, $N_r = 100$, and $N \to \infty$. The numerical results are shown as the thick black line. The analytical results for $N_r \equiv 1$, Eq. (5), are plotted as $\sigma_{CL}(\gamma)$ (red circles) and $\sigma_{CL}(N_r\gamma)$, i.e., the horizontal axis is scaled with N_r (blue squares). The inset shows the dependence of σ on $N - 2N_r$ at $\gamma = 0.1\sqrt{mK}$.

flowing from left to right is $J_{L\to R} = k_B T_L l_L^{-1} \sum_{q>0} v_q$, where v_q is the group velocity of a phonon with momentum q (restricted to phonons moving to the right, i.e., $q > 0$), k_B is Boltzmann's constant, and l_L is the length of the left lattice. Essentially, this expression is just the amount of classical energy stored in a specific phonon mode in equilibrium ($k_B T_L$), multiplied by its group velocity (v_q) and the local phonon density of states ($1/l_L$). Similarly introducing $J_{R\to L}$, taking the limit $l_L, l_R \to \infty$, and defining the total current as $J = J_{L\to R} - J_{R\to L}$, we obtain the intrinsic conductance as

$$\sigma_2 \equiv \frac{J}{\Delta T} = \frac{k_B}{2\pi}\int_\Omega dq\, v_q = \frac{k_B}{2\pi}\int_\Omega dq\, \frac{d\omega(q)}{dq} = \frac{k_B\Omega}{2\pi}, \quad (2)$$

where $\Omega = \omega_{\max} - \omega_{\min}$ is the phonon bandwidth. This conductance is also expressible as $\sigma_2 = \bar{v}_q/2$, where $\bar{v}_q$ is the group velocity averaged over the entire band, which gives additional insight into its form. The eigenmodes of the Hamiltonian, Eq. (1), obey $\omega^2 = \left[D + 4K\sin^2(q/2)\right]/m$, so that $\omega_{\min} = \sqrt{D/m}$, $\omega_{\max} = \sqrt{(D+4K)/m}$, and, therefore, the phonon bandwidth is

$$\Omega = \sqrt{\frac{K}{m}}\left[\sqrt{D/K + 4} - \sqrt{D/K}\right]. \quad (3)$$

Accordingly, the intrinsic conductance becomes

$$\sigma_2 = \frac{k_B}{2\pi}\sqrt{\frac{K}{m}}\left[\sqrt{D/K + 4} - \sqrt{D/K}\right]. \quad (4)$$

The intrinsic conductance is the maximum possible conductance of a harmonic system between two equilib-

rium reservoirs at different temperatures: No matter how much energy the reservoirs can pump into the system, the free lattice itself can not usher the energy from source (L) to sink (R) faster than the rate allowed by its intrinsic conductance. The magnitude of σ_2 is plotted in Fig. 2 (thin dashed line), showing an excellent agreement with the numerically calculated conductance in regime (2) (hence the subscript of σ_2). We also note that decreasing D – the onsite confining potential – and holding all other factors fixed increases the conductance, an effect that is observed in models of DNA denaturation [19, 20]. This is purely due to the increasing bandwidth.

Casher-Lebowitz formula. The other two regimes, (1) and (3), become physically transparent when using the Casher-Lebowitz formula [15] for a *single-site reservoir* at each end (i.e., $N_r \equiv 1$)

$$\sigma_{CL}(\gamma) = \frac{k_B\gamma}{2\pi m}\int_0^{2\pi} dq\, \frac{\sin^2 q}{1+\frac{2\gamma^2}{mK}\left[1+\frac{D}{2K}-\cos q\right]}. \quad (5)$$

It is readily seen that the small and large γ expansion of the expression yields $\sigma_{CL} \propto \gamma$ and $\sigma_{CL} \propto 1/\gamma$, respectively. In fact, very general perturbative arguments suggest that these $\sigma \propto \gamma$ and $\sigma \propto 1/\gamma$ regimes are generic for arbitrary harmonic lattices, as we show in the supplementary information.

Equation (5) is plotted in Fig. 2 as a function of two different arguments: the bare friction coefficient, $\sigma_{CL}(\gamma)$ (red circles), and the scaled friction coefficient, $\sigma_{CL}(N_r\gamma)$ (blue squares). As is seen in the figure, they coincide with numerical results at large and small γ, respectively, which we will now explain.

Small γ regime. The small γ expansion of Eq. (5) is $\sigma_{CL} = \frac{k_B\gamma}{2\pi m}\int_0^{2\pi} dq\, \sin^2 q = \frac{k_B\gamma}{2m}$. This expression reflects the fact that energy is pumped in/out of the system via the end sites at a rate proportional to γ, and this rate is much smaller (at small γ) than the one the free lattice can carry *intrinsically*, σ_2. At these conditions (i.e., $k_B\gamma/m \ll \sigma_2$), the heat input by the noise term in Eq. (14) is so inefficient that the system has enough time to equilibrate at some global temperature T'. In this quasi-equilibrium state the noise-induced heat current entering the left reservoir is $J_L = \frac{\gamma}{m}k_B(T_L - T')$, and similarly for the right reservoir $J_R = \frac{\gamma}{m}k_B(T_R - T')$. At the steady state $J = J_L = -J_R$, which yields $T' = \frac{T_L+T_R}{2}$, so that the conductance of the entire system becomes $\sigma = \frac{k_B\gamma}{2m}$, in full agreement with the small-γ expansion of Eq. (5) above.

These quasi-equilibrium-based considerations can be straightforwardly generalized to the case of extended reservoirs of arbitrary size N_r yielding

$$\sigma_1(\gamma) = \frac{k_B N_r\gamma}{2m} \equiv \frac{k_B\Gamma}{2m}, \quad (6)$$

i.e., the heat is pumped into the system at a rate proportional to cumulative friction constant $\Gamma = N_r\gamma$. This is the reason why Casher-Lebowitz formula (5), once plotted as a function of the *cumulative* friction constant, $\sigma_{CL}(N_r\gamma)$, coincides with the numerical results in Fig. 2 at small γ. The agreement between Eq. (6) and numerical results in the weak friction regime is emphasized in Fig. 3 where conductances for a range of N_r exactly overlaps with $k_B\Gamma/2m$ at small friction.

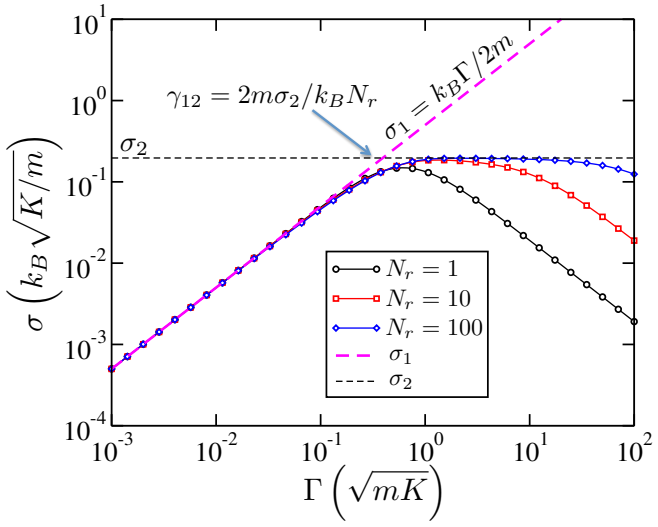

FIG. 3. Comparison of numerical (circles, square, diamonds) and analytical results (dashed lines) in the small Γ regime at $D/K = 1$ for different sizes of extended reservoirs, N_r.

Eq. (6) is only valid at sufficiently small Γ. When $\frac{k_B\Gamma}{2m}$ becomes higher than σ_2, the free lattice cannot transfer all the heat the Langevin reservoirs are able to supply. At that point, i.e., $\gamma \approx \gamma_{12} = 2m\sigma_2/k_BN_r$ (marked in Figs. 2 and 3), the conductance of the overall system levels off and regime (2) is established.

Large γ regime. The large γ expansion of Eq. (5) is

$$\sigma_3 = \frac{k_BK}{2\gamma}\left(1 - \frac{\sqrt{mD}}{2K}\Omega\right). \quad (7)$$

At large γ, the noise term in Eq. (14) can efficiently supply heat to a lattice site. However, this site is effectively decoupled from the adjacent sites since the very large friction *overdamps* its motion resulting in the reservoir site becoming "off-resonant" from the rest of the lattice. We will discuss this in detail in the next section. Heuristically, however, the efficiency of heat transfer from the reservoir site to the free lattice has to be proportional to a phonon group velocity and to a time the reservoir site can stay coherent with the rest of the lattice. The latter is given by the decoherence time of an overdamped oscillator, $1/\gamma$, so the conductance becomes (averaging over all phonon modes) $\sigma_3 \propto \frac{1}{\gamma}\int_\Omega d\omega\, v_q(\omega)$. This coincides with Eq. (7) up to a constant prefactor.

This heuristic argument is directly applicable to the case of extended reservoirs ($N_r > 1$). Indeed, the reservoir site directly connected to the free lattice is the one that excites phonons in the free lattice and the remain-

ing $N_r - 1$ reservoir sites (on the left or on the right) are decoupled from the lattice by at least another order of $1/\gamma$. This entails that the heat conductance is independent of N_r in the large-γ regime, which agrees with the numerical results in Fig. 2. When $\sigma_3(\gamma)$ reaches σ_2 as γ decreases to $\gamma \approx \gamma_{23} = \frac{k_B K}{2\sigma_2}\left(1 - \frac{\sqrt{mD}}{2K}\Omega\right)$ (marked in Fig. 2), there is a crossover from regime (3) to (2). That is, as γ decreases the reservoir site becomes coherent enough to efficiently transfer heat to the free lattice, so the finite intrinsic conductance of the free lattice, σ_2, becomes the limiting factor.

The plateau and tilt. Regime (2) is just a crossover point at $N_r = 1$ [Eq. (5)], but it becomes a pronounced plateau at $N_r \gg 1$ as shown in Fig. 3. This is because the position of the crossover between regimes (2) and (3), γ_{23}, does not depend on N_r, but the one between regimes (1) and (2), does as $\gamma_{12} \propto 1/N_r$. At sufficiently large N_r the two crossovers are thus well separated, establishing a plateau in between.

Closer inspection of the numerical results reveals that the "plateau" is in fact tilted, see Fig. 4. The linear fit of this tilted plateau yields an intercept with the $\gamma = 0$ axis numerically close to σ_2 and the slope independent (within the fitting accuracy) of any parameters of the lattice.

We demonstrate below that once $N_r \to \infty$, the conductance becomes σ_2 as $\gamma \to 0$ (the order of taking the two limits is important: the limit of $N_r \to \infty$ is assumed to be taken first, i.e., $\Gamma = N_r\gamma \to \infty$). When γ is finite, though, the conductance falls off linearly with γ with a *universal* slope. This tilt can be understood via the inhomogeneity of the lattice. For example, connecting lattices that have only partially overlapping phonon bands results in a poor conductance due to scattering at the interfaces [21]. In our situation, the phonons in the extended reservoirs and the free lattice are *different* because of a finite phonon lifetime in the former (due to friction) and an infinite lifetime in the latter. Within the extended reservoir, each phonon has a spread in frequency $\delta\omega \approx \gamma$. This smearing results in imperfectly overlapping bands at the band edges, which in turn leads to a decreasing conductance as γ increases.

The more rigorous understanding of the tilt can be achieved by considering phonon scattering at the interface between a free lattice and a lattice with uniform friction γ (K and D are the same for both). For a phonon of frequency ω incoming from the free lattice, the solution within the free lattice is $x_n(t) = e^{iqn-i\omega t} + Ae^{-iqn-i\omega t}$, where A is the reflection amplitude. The solution in the lattice with friction is $x_n(t) = Be^{iq'n-i\omega t}$, where q' has a non-zero imaginary component due to the finite phonon lifetime. Imposing the boundary conditions, the reflection amplitude is

$$A(q) = -\frac{1 - e^{-i(q'-q)}}{1 - e^{-i(q'+q)}}, \tag{8}$$

where $\cos q' = \cos q - i\gamma\omega/2K$ and $\omega = \omega(q)$ is the phonon dispersion relation for a free lattice. The two limiting cases are $A = 0$ at $\gamma \to 0$ and $|A| = 1$ at $\gamma \to \infty$ with $0 < |A| < 1$ at any finite γ. This justifies the heuristic argument above that phonons with and without friction are indeed different resulting in a finite reflection amplitude at the friction/frictionless interface. At finite γ, the reflection is most significant near the band edges (i.e., within $\delta\omega \approx \gamma$ of $\omega_{\min}$ or $\omega_{\max}$).

In equilibrium at temperature T, the momentum-resolved current from the free lattice to the extended reservoir is $J(q) = k_B T v_q [1 - R(q)]$ for $q > 0$, where $R(q) = |A(q)|^2$ is the reflection coefficient. It is difficult to directly evaluate the current from the extended reservoir to the free lattice, but in equilibrium this current has to fully compensate the one entering the reservoir from the free lattice. Using this correspondence, we can now write down the current from a reservoir to the free lattice even at non-equilibrium conditions. This results in the following set of balance equations for the heat current through a free lattice between two extended reservoirs,

$$\begin{aligned} J_L(q) - R(q)J(-q) &= J(q), \\ J_R(-q) - R(q)J(q) &= J(-q), \end{aligned} \tag{9}$$

where $J(q)$ is the current within the free lattice and $J_{L(R)}$ is the current from the left (right) reservoirs. For example, the first equation states that the current from left to right within the free lattice equals the current from the left reservoir plus the portion of "left" current, $J(-q)$, reflected by the interface with the right reservoir. Solving these equations and integrating over all phonon modes, $\int_0^\pi dq\, [J(q) + J(-q)]$, we obtain

$$\sigma(\gamma) = \frac{k_B}{2\pi}\int_0^\pi dq\, v_q \frac{1 - R(q)}{1 + R(q)}, \tag{10}$$

which is similar to Eq. (2), except for the quotient within the integrand. This quotient is strictly positive and always less than 1 – it represents the non-vanishing thermal resistance of the interfaces due to phonon scattering and is known as the Kapitza resistance [22]. The small-γ expansion of Eq. (10) produces a very simple result

$$\sigma(\gamma) \approx \sigma_2 - \frac{\pi}{48}\frac{k_B\gamma}{m}, \tag{11}$$

shown in Fig. 4 by blue crosses. As is seen, the universal tilt of $-\pi k_B/48m$ is independent of lattice parameters (except for mass) and in excellent agreement with numerical results in the plateau region. Furthermore, it turns out that Eq. (10) evaluated at arbitrary γ (red circles) does not only exactly reproduce the tilted plateau but also the high-γ regime (3). In particular, the large-γ expansion of Eq. (10) results in Eq. (7). Therefore, Eq. (10) is *exact* in the limit of $N_r \to \infty$ and is valid for the "moderate to strong friction" regime. The only regime it cannot reproduce is regime (1) since the limit $N_r \to \infty$ has been taken in the scattering calculation,

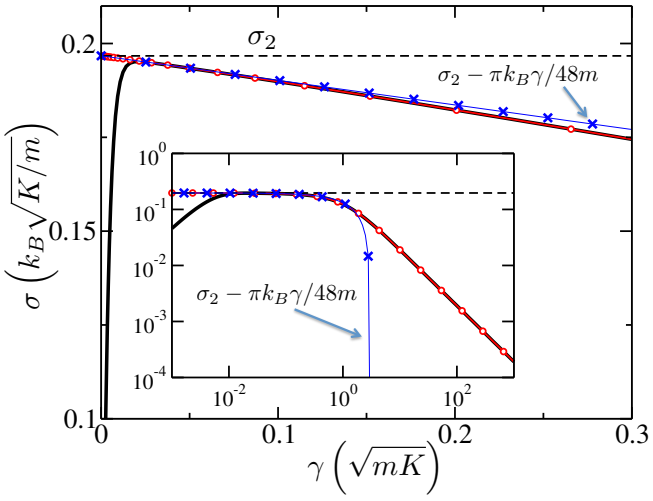

FIG. 4. Comparison of the exact numerical results (thick black line) for the conductance with the semi-analytical result, Eq. (10), shown by red circles. The model parameters are $D/K = 1$ and $N_r = 100$. Thin dashed line shows σ_2. The inset shows that the semi-analytic result also works in the large γ regime. For weak friction, Eq. (10) reduces to Eq. (11), shown by blue crosses.

which stretches the plateau all the way to $\gamma = 0$.

Kramers' theory. The crossover behavior discussed above is the thermal transport analog of the Kramers' theory for the classical transition rate of a particle out of a metastable well in the presence of friction and noise [23, 24], as depicted in Fig. 1(b) for a double-well potential. The rate constant for the transition is $k(E_b, \gamma) = k_0(\gamma)e^{-E_b/k_BT}$, where E_b is the height of the energy barrier and the prefactor $k_0(\gamma)$ depends on γ. Kramers demonstrated that $k_0(\gamma) \sim \gamma$ when γ is small. In general, the energy supplied by the noise to a particle in a certain well is lost either to friction or to the particle leaving this well by overcoming the barrier. The latter energy loss channel dominates when γ is very small so the friction can be essentially neglected. At these conditions, the transition rate is limited by the low rate at which noise can supply energy needed for a particle to overcome the barrier. This rate is linear with respect to γ, resulting in $k_0(\gamma) \sim \gamma$. This behavior is indeed analogous to regime (1) in the thermal transport problem, where the free lattice is very efficient in carrying heat, so the heat current is limited by the rate at which the Langevin reservoir can input energy into the system, Eq. (6).

On the other extreme, as γ becomes very large, Kramers showed that $k_0(\gamma) \sim 1/\gamma$. In this regime, the dynamics of the particle in the Kramers' problem becomes increasingly non-ballistic due to the strong friction and noise. This results in the high probability of *re-crossings*, i.e., even if the particle overcomes the barrier and crosses the surface separating the wells, the very strong noise can still push it back thus preventing its thermalization in the new potential well [24]. The probability of re-crossings grows with γ resulting in $k_0(\gamma) \sim 1/\gamma$.

In order to illustrate the re-crossing phenomenon in the Kramers' problem and emphasize its similarity to the large-γ regime (3) of the thermal transport problem, we deform the barrier in the Kramers' problem as shown in Fig. 1(c). Specifically, we "stretch" the very top of the barrier into a horizontal *ballistic* region (i.e., no friction/noise) of a finite length (this is in contrast with the example of Section VII.E of Ref. [23], where dissipation is present everywhere). This modification does not affect the transition rate since if a particle enters this region with a certain velocity, it will leave this region with the same velocity (remember that, within our model, there is no friction in the horizontal region). The only thing that changes by adding this "stretching" is the time required for a particle to cross the barrier – irrelevant in the steady state.

Once a particle reaches the top of the barrier going from the left, it propagates freely along the ballistic region until it reaches the onset of the right well. Upon hitting this onset, the particle immediately becomes subject to noise which, if strong enough, can kick it back to the ballistic region, so the particle might end up in the the well it originally came from. Thus, the particle can be thought of as being *reflected* off the boundary between ballistic and non-ballistic regions. This is the phenomenon of re-crossing – the top of the barrier can be crossed multiple times without thermalization in either of the potential wells.

This perspective demonstrates the analogy to thermal transport at "moderate to strong" γ. Indeed, we were able to describe the thermal transport in regime (2) and regime (3), see inset in Fig. 4, by considering *reflections* of phonons off the boundary between the free lattice (no friction) and one of the reservoirs (friction is present). The ballistic region and the two potential wells in the deformed double-well potential are then respective analogs of the free lattice and the extended reservoirs in the thermal transport problem.

This deep physical similarity between the two problems, when looked upon from the perspective of particle (or phonon) reflection, calls for qualitatively similar behavior as the magnitude of friction varies. Indeed, Eq. (10) gives $\sigma \sim 1/\gamma$ at large γ, which matches $k_0(\gamma) \sim 1/\gamma$ in Kramers' problem. Furthermore, at intermediate values of γ, the general Kramers' solution reduces to the transition state theory (TST) rate $k_{\rm TST}$ which does not depend on γ [23, 24]. More accurately, the Kramers' rate equals to $k_{\rm TST}$ with negative corrections linear with respect to γ, so that $k_{\rm TST}$ is always an exact upper limit of the Kramers' rate. This happens as well in the thermal transport problem where the conductance in regime (2) is given by Eq. (11). In this equation, σ_2 – an exact upper limit – is an *intrinsic* conductance of the free lattice, which does not depend on friction.

We note that similar arguments can be applied to a version of the Kramers' problem where a classical par-

ticle escapes a single metastable potential well [23]. In this formulation, Kramers' problem becomes analogous to a problem of thermal transport through the interface between a free lattice and a lattice with uniform friction studied by us when discussing the tilt of the plateau. In particular, the low probability of phonon transmission through the interface between these two lattices at large γ is analogous to the particle escape rate scaling as $1/\gamma$ in the Kramers' problem of a metastable potential well.

The appealing picture developed above is based on very general and intuitive physical arguments and is, therefore, expected to be valid beyond the specific case of a uniform harmonic lattice. Indeed, below we discuss the two important cases of (i) a harmonic lattice with disorder and (ii) an anharmonic lattice. We demonstrate the existence of three distinct regimes of thermal transport and, therefore, the similarity to Kramers' problem.

Disordered Harmonic Lattice. The Hamiltonian for a harmonic lattice with mass disorder reads as

$$H = \frac{1}{2}\sum_{n=1}^{N} m_n \dot{x}_n^2 + \frac{D}{2}\sum_{n=1}^{N} x_n^2 + \frac{K}{2}\sum_{n=0}^{N}(x_n - x_{n+1})^2. \quad (12)$$

The mass disorder is realized by sampling mass uniformly and independently for each lattice site within the interval $m_n = m \pm \delta m = m(1.0 \pm 0.3)$, so that the mean mass, m, is the same as in the non-disordered case, Eq (1). The central "free" part of the lattice is kept to be $N - 2N_r = 60$ sites long. The sizes of the extended reservoirs are N_r =1, 10 and 100 (the same on the left and on the right in each calculation).

Figure 5(a) shows the heat conductance versus γ for a harmonic lattice with mass disorder. The presented numerical results are statistically averaged over the disorder. The crossover behavior is indeed present. Furthermore, when N_r increases the plateau starts to form as it was the case for the homogeneous lattice. However, the magnitude of the conductance at the plateau, σ_2(dis), is approximately an order of magnitude lower than σ_2(hom) (dashed black line), the latter being the intrinsic conductance of the homogeneous lattice. This is due to disorder-induced finite phonon mean free path being shorter than $N - 2N_r = 60$, which lowers the conductance.

Anharmonic Lattice. To investigate the crossover behavior in an anharmonic lattice we examine the thermal conductance in a paradigmatic nonlinear lattice – the Peyrard-Bishop-Dauxois (PBD) model [25–27]. The PBD model is a one dimensional lattice that represents nonlinear fluctuations of DNA as it denatures. Here, we are primarily interested in the crossover behavior for a highly nonlinear lattice, rather than the physics of the denaturation transition where the double helix separates into two single strands (the transport physics described by this model has been discussed elsewhere, see

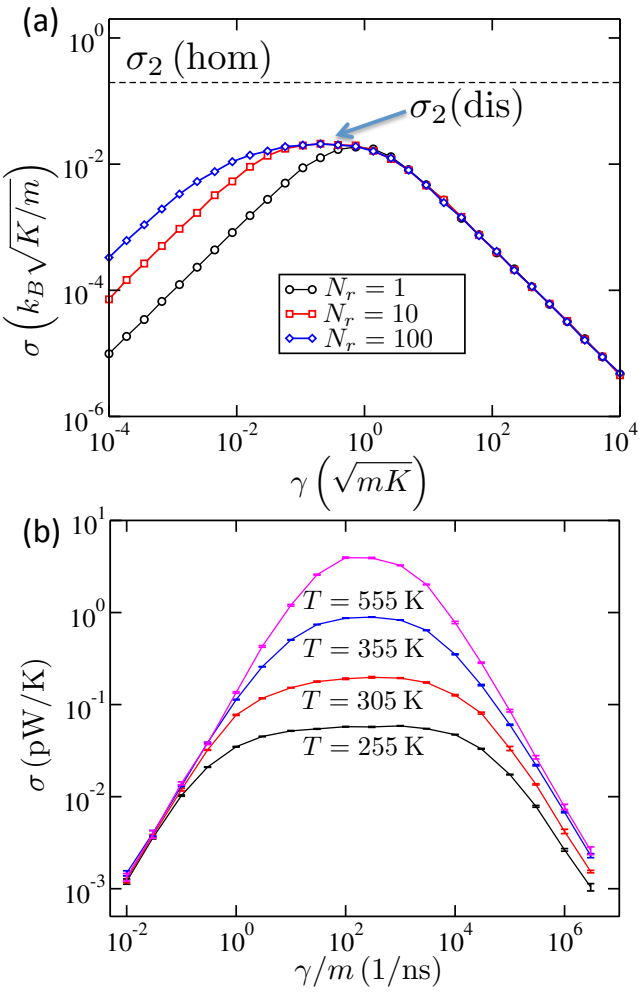

FIG. 5. Crossover behavior in disordered and anharmonic lattices. (a) The thermal conductance of a disordered harmonic lattice with N_r =1, 10 and 100 (black circles, red squares and blue diamonds) and $N - 2N_r = 60$. The system is the same as that in Fig. 2, i.e., $D/K = 1$, except for the mass which is now sampled uniformly and independently for each site within the interval $m_n = m(1\pm0.3)$. The dashed line gives the intrinsic conductance for a homogeneous lattice, σ_2(hom), demonstrating that the disorder significantly decreases the heat conductance of the lattice, σ_2(dis) at the plateau. The curve is averaged over 100 to 1000 realizations of the disorder so that magnitude of the error due to the incomplete averaging over disorder is comparable to the thickness of the lines. (b) The thermal conductance of anharmonic PBD lattice with $N_r = 20$ and $N = 100$ for various average temperatures T. The error bars are computed using the range of fluctuations of the cumulative current for the final 10 % of the simulation time.

Refs. [19, 20]). The Hamiltonian takes on the form

$$H = \frac{1}{2}\sum_{n=1}^{N} m\dot{x}_n^2 + \sum_{n=1}^{N} V(x_n) + \sum_{n=0}^{N} W(x_n, x_{n+1}), \quad (13)$$

where x_n represents the base-to-base distance within the

n^{th} base pair. The on-site Morse potential $V(x_n) = \tilde{D}(e^{-ax_n}-1)^2$ represents the hydrogen bonding between the bases and the coupling term $W(x_n, x_{n+1}) = \frac{\tilde{K}}{2}(1+\rho e^{-b(x_n+x_{n+1})})(x_n - x_{n+1})^2$ gives the stacking interaction. We note that with small amplitude fluctuations (at low temperature) this model is harmonic with parameters $D = 2\tilde{D}/a^2$ and $K = \tilde{K}(1+\rho)$. Similarly, at high temperature, the model is harmonic with parameters $D = 0$ and $K = \tilde{K}$. In between, the model displays highly nonlinear behavior.

The results of simulations, shown in Fig. 5(b), clearly demonstrate three regimes of thermal transport. Specifically, $\sigma(\gamma) \sim \gamma$ and $\sigma(\gamma) \sim 1/\gamma$ at small and large γ, respectively. Regime (2), where $\sigma(\gamma) \approx$ constant, is most pronounced at lower temperatures because the extended reservoir size is kept fixed and the conductance is lowest at this point, see the discussion below. We have shown elsewhere that this regime has a well-defined conductivity [20].

Unlike the harmonic model, the intrinsic conductance of nonlinear lattices does in general depend on temperature. In case of the PBD model, the intrinsic conductance of the lattice increases as the average temperature increases across the denaturation transition, which is apparent in the increase of the conductance plateau. This increase is due to the decrease in nonlinearity of the model as the transition is crossed from below. Moreover, the length of the plateau region shortens due to the increasing conductance. At higher temperatures, the crossover from Regime (1) to Regime (2) happens at a larger γ, as the rate of heat input from the reservoir ($\sim \gamma$) has to compete with the intrinsic conductance of the complete reservoir/lattice system. A similar shift in the crossover happens for Regime (2) to Regime (3). In addition to this model, the crossover behavior has been observed in other anharmonic lattices, such as the FPU lattice [5]. We note that for anharmonic lattices the heat conductance can scale nontrivially with the length and temperature, which will result in an intricate interplay between these variables, the extended reservoir size, and the width of the plateau region, as seen in Fig. 5(b).

DISCUSSION

We elucidated the mechanisms behind the crossover behavior of thermal transport as the strength of coupling to the reservoirs is varied. The evidence suggests that this behavior is universal, applying to harmonic, anharmonic, and disordered systems. It is also guaranteed to exist in higher dimensional harmonic systems as well, due to the closed form expression of transport in arbitrary lattices. This phenomenon parallels the physical behavior observed in Kramers' transition state problem. Our results illuminate the regime where the intrinsic conductance is manifest. It is in this regime where nonlinear fluctuations, disorder, etc., dominate the conductance and where thermal transport can be used to probe physical processes, such as DNA denaturation [19, 20]. We also note that in many physical systems, the friction coefficient γ depends on frequency, giving rise to memory in the equations of motion [13, 18, 28]. We expect a crossover to still occur when the overall coupling to the external reservoirs is tuned. The intermediate regime, however, may display more complex behavior due to how the reservoirs affect modes at different frequency scales. We leave this study for a future investigation.

Moreover, non-equilibrium molecular dynamic simulations is the standard tool in the study of thermal transport in nanoscale systems (see, e.g., refs [3, 29–36]). In these simulations the strength of coupling to the environment (in the form of, e.g., Langevin or Nose-Hoover thermostats) is a free parameter. It is relatively innocuous when a well-defined conductivity exists. However, when both ballistic and diffusive effects are present – as is the case at the nanoscale – the choice of this coupling affects the calculation of the thermal conductance. It thus must be chosen to appropriately simulate the property of interest, whether it is the thermal conductance of the device or the intrinsic conductance of the functional system. This is especially important when extracting scaling exponents of the conductance versus temperature or lattice length in nonlinear and disordered systems, as both quantities nontrivially affect the conductance and the crossover behavior can spuriously influence the predicted scaling.

METHODS

Harmonic Lattices. The harmonic lattices we consider are described by Eq. (1). We also connect two additional sites x_0 and x_{N+1} to the ends of the lattice, which are fixed at zero. The Langevin equations of motion are

$$m\ddot{x}_n + Dx_n + K[2x_n - x_{n-1} - x_{n+1}] = f_n(t), \quad (14)$$

where the l.h.s. describes the Hamiltonian dynamics and the r.h.s. is the reservoir-induced noise and friction forces, $f_n(t) = \eta_n(t) - \gamma_n \dot{x}_n(t)$. The noise $\eta_n(t)$ and friction coefficient γ_n are related by the fluctuation-dissipation relation

$$\langle \eta_n(t)\eta_m(t')\rangle = 2\gamma_n k_B T_n \delta_{nm}\delta(t-t'). \quad (15)$$

The three regions of the lattice (L, F and R) are encoded in equations of motion by setting

$$\gamma_n = \begin{cases} \gamma, & n \in L \text{ or } R \\ 0, & n \in F \end{cases} \quad (16)$$

and $T_n = T_L$ or T_R for $n \in L$ or R, respectively. Here, a collection of independent (uncorrelated) single site Langevin reservoirs approximates the contact to the thermal reservoir [37]. When $T_L = T_R = T$, the lattice will relax into an equilibrium state at temperature T, as guaranteed by the fluctuation-dissipation theorem.

When $T_L \neq T_R$, a heat current will flow (we assume $T_L > T_R$ without loss of generality).

The current flowing from site n to $n+1$ is given by [15, 37]

$$J_n = K\langle \dot{x}_{n+1} x_n \rangle, \tag{17}$$

where the average is over the statistical ensemble. For $n \in F$, J_n will be independent of n, i.e., $J_n \equiv J$, in the steady state.

We note that thermal transport occurs ballistically in a frictionless harmonic lattice. This results in a diverging *conductivity*, which can be defined as $\lim_{N\to\infty}(N-2N_r)\sigma$ at fixed N_r. However, the conductance, σ, is well defined and is rapidly converging to its value corresponding to an infinite lattice, as shown in the inset of Fig. 2. Henceforth, we always assume $N \to \infty$ at fixed N_r for homogeneous harmonic lattices. Dimensional analysis shows that the conductance of a uniform harmonic lattice in the limit $N \to \infty$ takes the form (see the Supplementary Information for the derivation)

$$\sigma = \frac{J}{\Delta T} = k_B \sqrt{\frac{K}{m}} C\left(\frac{D}{K}, \frac{\gamma}{\sqrt{mK}}, N_r\right), \tag{18}$$

where $\Delta T = T_L - T_R$ and C is a as of yet unknown dimensionless function of three dimensionless arguments. This expression implies that harmonic lattices with distinct values of parameters are nevertheless physically similar if $\sqrt{K/m}$, D/K, $\gamma/\sqrt{mK}$, and N_r are identical. Such models can be said to form a "similarity class". In what follows, all the figures pertaining to the harmonic case are plotted in natural units, i.e., γ is plotted in units of $\sqrt{mK}$, σ is plotted in units of $k_B\sqrt{K/m}$, etc. Note that we use ΔT defined with the external reservoir temperatures T_L and T_R, as these are the ones typically set/measured experimentally.

For the anharmonic lattice, the setup is the same as for harmonic lattices, but with the equation of motion given by its respective Hamiltonian.

Numerical Methods. For anharmonic lattice the evolution of the coordinates is computed using the Brünger-Brooks-Karplus integrator with a time step of 10 fs. The total length of the simulation varies from 0.1 ms to 2 ms depending on the convergence of current. The temperature difference between the hot and cold reservoirs was maintained at 9.3K for all calculations. The parameters used are same as in Ref. [26], i.e., $\tilde{D} = 0.04$ eV, $a = 44.5$ nm^{-1}, $\tilde{K} = 4$ eV/nm^2, $\rho = 0.5$, $b = 3.5$ nm^{-1}, and $m = 300$ u.

[1] Li, N. *et al. Colloquium*: Phononics: Manipulating heat flow with electronic analogs and beyond. *Rev. Mod. Phys.* **84**, 1045–1066 (2012).

[2] Dubi, Y. & Di Ventra, M. Colloquium: Heat flow and thermoelectricity in atomic and molecular junctions. *Rev. Mod. Phys.* **83**, 131 (2011).

[3] Yang, N., Xu, X., Zhang, G. & Li, B. Thermal transport in nanostructures. *AIP Advances* **2**, 041410 (2012).

[4] Bonetto, F., Lebowitz, J. & Rey-Bellet, L. Fourier's law: A challenge for theorists. In Fokas, A., Grigoryan, A., Kibble, T. & Zegarlinski, B. (eds.) *Mathematical Physics 2000*, 128 (Imperial College Press, London, UK, Chicago, 2000).

[5] Lepri, S., Livi, R. & Politi, A. Thermal conduction in classical low-dimensional lattices. *Phys. Reports* **377**, 1–80 (2003).

[6] Dubi, Y. & Di Ventra, M. Fourier's law: Insight from a simple derivation. *Phys. Rev. E* **79**, 042101 (2009).

[7] Michel, M., Gemmer, J. & Mahler, G. Microscopic quantum mechanical foundation of Fourier's law. *Int. J. Mod. Phys. B* **20**, 4855–4883 (2006).

[8] Buchanan, M. Heated debate in different dimensions. *Nature Phys.* **1**, 71–71 (2005).

[9] Li, Y., Liu, S., Li, N., Hanggi, P. & Li, B. 1D momentum-conserving systems: The conundrum of anomalous versus normal heat transport. *New J. Phys.* **17**, 043064 (2015).

[10] Fermi, E., Pasta, J. & Ulam, S. Studies of the nonlinear problems. I. *Los Alamos Sci. Lab. Rep. No. LA-1940* (1955).

[11] Berman, G.P. & Izrailev, F. M. The Fermi–Pasta–Ulam problem: 50 years of progress. *Chaos* **15**, 015104 (2005).

[12] Gallavotti, G. *The Fermi-Pasta-Ulam problem: a status report*, vol. 728 (Springer Verlag, 2008).

[13] Dhar, A. Heat transport in low-dimensional systems. *Adv. Phys.* **57**, 457–537 (2008).

[14] Liu, S., Xu, X., Xie, R., Zhang, G. & Li, B. Anomalous heat conduction and anomalous diffusion in low dimensional nanoscale systems. *Eur. Phys. J. B* **85**, 1–20 (2012).

[15] Casher, A. & Lebowitz, J. L. Heat flow in regular and disordered harmonic chains. *J. Math. Phys.* **12**, 1701–1711 (1971).

[16] Bernardin, C. & Olla, S. Fouriers law for a microscopic model of heat conduction. *J. Stat. Phys.* **121**, 271–289 (2005).

[17] Nakazawa, H. On the lattice thermal conduction. *Prog. Theor. Phys. Supplement* **45**, 231–262 (1970).

[18] Dhar, A. Heat conduction in the disordered harmonic chain revisited. *Phys. Rev. Lett.* **86**, 5882 (2001).

[19] Velizhanin, K. A., Chien, C.-C., Dubi, Y. & Zwolak, M. Driving denaturation: Nanoscale thermal transport as a probe of DNA melting. *Phys. Rev. E* **83**, 050906 (2011).

[20] Chien, C.-C., Velizhanin, K. A., Dubi, Y. & Zwolak, M. Tunable thermal switching via DNA-based nano devices. *Nanotechnology* **24**, 095704 (2013).

[21] Terraneo, M., Peyrard, M. & Casati, G. Controlling the Energy Flow in Nonlinear Lattice: A model for a Thermal Rectifier. *Phys. Rev. Lett.* **88**, 094302 (2002).

[22] Kapitza, P. L. The study of heat transfer in helium II. *J. Phys.(USSR)* **4**, 181-201 (1941).

[23] Hänggi, P., Talkner, P. & Borkovec, M. Reaction-rate theory: Fifty years after Kramers. *Rev. Mod. Phys.* **62**, 251 (1990).

[24] Melnikov, V. I. The Kramers problem: Fifty years of

development. *Phys. Rep.* **209**, 1–71 (1991).

[25] Peyrard, M. & Bishop, A. R. Statistical mechanics of a nonlinear model for DNA denaturation. *Phys. Rev. Lett.* **62**, 2755–2758 (1989).

[26] Dauxois, T., Peyrard, M. & Bishop, A. R. Entropy-driven DNA denaturation. *Phys. Rev. E* **47**, R44–R47 (1993).

[27] Dauxois, T., Peyrard, M. & Bishop, A. R. Dynamics and thermodynamics of a nonlinear model for DNA denaturation. *Phys. Rev. E* **47**, 684–695 (1993).

[28] Banerjee, S. & Dhar, A. Classical limit of master equation for a harmonic oscillator coupled to an oscillator bath with separable initial conditions. *Phys. Rev. E* **73**, 067104 (2006).

[29] Luo, T. & Lloyd, J. R. Non-equilibrium molecular dynamics study of thermal energy transport in Au–SAM–Au junctions. *Int. J. Heat Mass Transfer* **53**, 1–11 (2010).

[30] Wang, Y., Ruan, X. & Roy, A. K. Two-temperature nonequilibrium molecular dynamics simulation of thermal transport across metal-nonmetal interfaces. *Phys. Rev. B* **85**, 205311 (2012).

[31] Zhang, Y., Barnes, G. L., Yan, T. & Hase, W. L. Model non-equilibrium molecular dynamics simulations of heat transfer from a hot gold surface to an alkylthiolate self-assembled monolayer. *Phys. Chem. Chem. Phys.* **12**, 4435–4445 (2010).

[32] Falat, T., Platek, B. & Felba, J. Non-equilibrium molecular dynamics simulation of heat transfer in carbon nanotubes - verification and model validation. Paper presented at *Thermal, Mechanical and Multi-Physics Simulation and Experiments in Microelectronics and Microsystems (EuroSimE), 2011 12th International Conference on*, 1–5, Linz. http://dx.doi.org/10.1109/ESIME.2011.5765853 (2011, April 18-20).

[33] Wang, S. C., Liang, X. G., Xu, X. H. & Ohara, T. Thermal conductivity of silicon nanowire by nonequilibrium molecular dynamics simulations. *J. Appl. Phys.* **105**, 014316 (2009).

[34] Saha, S. K. & Shi, L. Molecular dynamics simulation of thermal transport at a nanometer scale constriction in silicon. *J. Appl. Phys.* **101**, 074304 (2007).

[35] Xu, X. *et al.* Length-dependent thermal conductivity in suspended single-layer graphene. *Nature Comm.* **5** (2014).

[36] Mortazavi, B., Rajabpour, A., Ahzi, S., Rémond, Y. & Mehdi Vaez Allaei, S. Nitrogen doping and curvature effects on thermal conductivity of graphene: A non-equilibrium molecular dynamics study. *Solid State Commun.* **152**, 261–264 (2012).

[37] Segal, D., Nitzan, A. & Hanggi, P. Thermal conductance through molecular wires. *J. Chem. Phys.* **119**, 6840–6855 (2003).

ACKNOWLEDGEMENTS

K.A.V. was supported by the U.S. Department of Energy through the LANL/LDRD Program. Y.D. acknowledges support from the Israel Science Fund (grant No. 1256/14). S. Sahu acknowledges support under the Cooperative Research Agreement between the University of Maryland and the National Institute of Standards and Technology Center for Nanoscale Science and Technology, Award 70NANB10H193, through the University of Maryland.

CONTRIBUTIONS

M.Z. proposed the project and C.C.C. and M.Z. obtained an initial description of the crossover behavior. K.A.V. suggested the connection to Kramers problem and developed an elegant theory of the crossover. K.A.V., C.C.C., and M.Z. performed analytical calculations and S.S. and K.A.V. performed numerical calculations. All authors wrote the manuscript and clarified the ideas.

COMPETING FINANCIAL INTERESTS

The authors declare no competing financial interests.

Crossover behavior of the thermal conductance and Kramers' transition rate theory – Supplemental Information

Kirill A. Velizhanin,[1,*] Subin Sahu,[2] Chih-Chun Chien,[3] Yonatan Dubi,[4] and Michael Zwolak[2,5,†]

[1] *Theoretical Division, Los Alamos National Laboratory, Los Alamos, NM 87545, USA*
[2] *Department of Physics, Oregon State University, Corvallis, OR 97331, USA*
[3] *School of Natural Sciences, University of California, Merced, CA 95343, USA*
[4] *Department of Chemistry and the Ilse Katz Institute for Nanoscale Science and Technology, Ben-Gurion University of the Negev, Beer-Sheva 84105, Israel*
[5] *Center for Nanoscale Science and Technology, National Institute of Standards and Technology, Gaithersburg, MD 20899, USA*

I. DIMENSIONAL ANALYSIS OF THE UNIFORM HARMONIC MODEL

The complete list of parameters of the uniform harmonic model introduced in main article is: m, D, K, γ, k_BT_L, k_BT_R, N, N_r. We take m, K and $k_B\Delta T = k_B(T_L - T_R)$ as fundamental units to make all the other parameters dimensionless. Then, the independent dimensionless parameters of the model are

$$\frac{D}{K},\ \frac{\gamma}{\sqrt{mK}},\ \frac{T_L+T_R}{\Delta T},\ N \text{ and } N_r. \tag{1}$$

Using these dimensionless parameters, the *exact* expression for the heat current through the lattice can be written as

$$\frac{J}{k_B\Delta T}\sqrt{\frac{m}{K}} = C\left(\frac{D}{K}, \frac{\gamma}{\sqrt{mK}}, \frac{T_L+T_R}{\Delta T}, N, N_r\right), \tag{2}$$

where C is a dimensionless function of five dimensionless arguments. This very general expression can be simplified by (i) taking $N \to \infty$ (see inset in Fig. 2 of main article) and by (ii) exploiting the fact that the heat current in such a model is proportional to ΔT [see Eq. (17) and the related discussion], then the function C cannot depend on T_L and T_R. These considerations result in

$$\frac{J}{k_B\Delta T}\sqrt{\frac{m}{K}} = C\left(\frac{D}{K}, \frac{\gamma}{\sqrt{mK}}, N_r\right), \tag{3}$$

where C is now a dimensionless function of just three dimensionless arguments. The expression for heat conductance of the 1D uniform harmonic model considered in this work can then be written in the limit of $N \to \infty$ as

$$\sigma = k_B\sqrt{\frac{K}{m}}C\left(\frac{D}{K}, \frac{\gamma}{\sqrt{mK}}, N_r\right). \tag{4}$$

II. NUMERICAL SOLUTION OF LANGEVIN EQUATIONS OF MOTION

The Langevin equations of motion for a lattice of harmonic oscillators, given by the Hamiltonian

$$H = \frac{1}{2}\mathbf{p}^\intercal\mathbf{M}^{-1}\mathbf{p} + \frac{1}{2}\mathbf{x}^\intercal\mathbf{K}\mathbf{x}, \tag{5}$$

are a system of first-order linear differential equations

$$\begin{aligned}\dot{x}_n &= p_n/m_n,\\ \dot{p}_n + \sum_{m=1}^{N} K_{nm}x_m + \gamma_n p_n/m_n &= \eta_n(t),\end{aligned} \tag{6}$$

where the mass can potentially be site-dependent in order to, e.g., examine mass disorder, as discussed in main article. The matrix $\mathbf{K}$ contains the interaction potentials and $[\mathbf{M}]_{nm} = \delta_{nm}m_n$ is a diagonal matrix of the masses. These equations of motion can be expressed as

$$\frac{d}{dt}|q(t)\rangle + \mathbf{G}|q(t)\rangle = |\eta(t)\rangle, \tag{7}$$

where

$$|q\rangle \Rightarrow \begin{pmatrix}\vec{x}\\ \vec{p}\end{pmatrix}. \tag{8}$$

The non-symmetric matrix $\mathbf{G}$ is given by

$$\mathbf{G} = \begin{pmatrix}\mathbf{0} & -\mathbf{M}^{-1}\\ \mathbf{K} & \mathbf{\Gamma}\mathbf{M}^{-1}\end{pmatrix}, \tag{9}$$

where $\mathbf{\Gamma}$ is a diagonal matrix of the couplings to the Langevin reservoirs (and $\mathrm{tr}|\mathbf{\Gamma}| = 2\Gamma$, where Γ is the cumulative friction coefficient).

The formal solution of Eq. (7) is

$$|q(t)\rangle = \int_{t_0}^{t} dt'\, e^{-\mathbf{G}(t-t')}|\eta(t')\rangle. \tag{10}$$

An important class of observables can be expressed as an average of a quadratic form of $|q(t)\rangle$ over the statistical ensemble. For example, the heat current flowing from site n to site $n+1$ can be written as a statistical average

* kirill@lanl.gov
† mpz@nist.gov

of

$$J_n = -\frac{K_{n+1,n}}{m_{n+1}} p_{n+1} x_n. \tag{11}$$

An observable of this class can be represented by an operator $\mathbf{O}$ so that

$$\begin{aligned} O(t) &= \langle q(t)|\mathbf{O}|q(t)\rangle \\ &= \int_{t_0}^{t} dt' \int_{t_0}^{t} dt'' \, \langle \eta(t')|e^{-\mathbf{G}^\dagger(t-t')}\mathbf{O}e^{-\mathbf{G}(t-t'')}|\eta(t'')\rangle. \end{aligned} \tag{12}$$

Averaging over the statistical ensemble and using Eq. 15 from the methods section of main article for the autocorrelation function of the random forces, one obtains

$$O(t) = \int_{t_0}^{t} dt' \, \mathrm{Tr}\left[e^{-\mathbf{G}^\dagger(t-t')}\mathbf{O}e^{-\mathbf{G}(t-t')}\mathbf{F}\right], \tag{13}$$

where $\mathbf{F}$ is a diagonal matrix with its only non-zero elements given by

$$F_{N+n,N+n} = 2\gamma_n k_B T_n, \;\; n = 1, 2, ..., N. \tag{14}$$

The spectral decomposition of the particular class of non-symmetric operators $\mathbf{G}$ above necessarily includes left and right eigenvectors, i.e., $\mathbf{G} = \sum_k \lambda_k |k_R\rangle\langle k_L|$, where the components of right (column) and left (row) eigenvectors are denoted by $[|k_R\rangle]_n = v^R_{n,k}$ and $[\langle k_L|]_n = \left(v^L_{n,k}\right)^*$, respectively. The orthonormality condition is $\langle k_L|l_R\rangle = \sum_{n=1}^{2N}\left(v^L_{n,k}\right)^* v^R_{n,l} = \delta_{kl}$. The spectral decomposition of $\mathbf{G}^\dagger$ is given by $\mathbf{G}^\dagger = \sum_k \lambda_k^* |k_L\rangle\langle k_R|$, where $|k_L\rangle = \langle k_L|^\dagger$ and $\langle k_R| = |k_R\rangle^\dagger$.

Substituting these spectral decompositions into Eq. (13), setting $t_0 \to -\infty$ to find the steady-state value of the observable, and integrating, we obtain

$$O = \sum_{k,l=1}^{2N} \frac{\langle l_R|\mathbf{O}|k_R\rangle\langle k_L|\mathbf{F}|l_L\rangle}{\lambda_k + \lambda_l^*}. \tag{15}$$

This equation allows one to draw very general conclusions regarding the dependence of the observable O on temperature without the need to explicitly specify $\mathbf{G}$ and $\mathbf{O}$. Since operators $\mathbf{O}$ (e.g., heat current) and $\mathbf{G}$ do not typically depend on temperature, and the operator $\mathbf{F}$ in Eq. (14) is strictly linear with respect to temperature, O is then a linear form of $T_1, T_2, ..., T_N$. Specifically, since in the harmonic lattice case we examine there is only two independent temperatures, T_L and T_R, O is necessary a linear form of T_L and T_R, i.e.,

$$O(T_L, T_R) = \alpha_L T_L + \alpha_R T_R, \tag{16}$$

where α_L and α_R are coefficients that depend only on specific parameters of the system and the nature of operator $\mathbf{O}$, but not temperature. For example, since the heat current has to vanish at thermodynamic equilibrium, we must have $\alpha_L = -\alpha_R$ and, therefore,

$$J \propto T_L - T_R. \tag{17}$$

That is, the heat conductance depends only on the temperatures T_L and T_R through their difference. These considerations do not lead to the same conclusion in the case of anharmonic lattices, as illustrated in Fig. 5(b).

III. HEAT CURRENT IN 1D HARMONIC LATTICES

To use Eq. (15) to evaluate the heat current in the lattice of harmonic oscillators, one needs to construct operators $\mathbf{G}$ and $\mathbf{O}$. Below we explicitly construct these matrices and derive an expression for the heat current.

The system under consideration is a lattice of harmonic oscillators with only nearest neighbor coupling, which yields a matrix $\mathbf{K}$ in Eq. (5) that is sparse. For an oscillator with index n somewhere inside the lattice (i.e., $1 < n < N$), the corresponding n^{th} row of the matrix has only three non-zero components $(K_{n,n-1}, K_{n,n}, K_{n,n+1}) = (-K, D+2K, -K)$, where K and D are parameters in the Hamiltonian. The end sites, $n = 1$ and $n = N$, are assumed to be coupled to "hard walls", i.e., to implicit oscillators with indices $n = 0$ and $n = N+1$, respectively, whose coordinates are kept zero. This results in only two non-zero matrix elements in the very first and the very last rows of matrix $\mathbf{K}$: $(K_{1,1}K_{1,2}) = (D+2K, -K)$ and $(K_{N,N-1}K_{N,N}) = (-K, D+2K)$.

According to Eq. (11), the operator $\mathbf{J}_n$ corresponding to the heat current from site n to site $n+1$ has only a single non-zero element

$$[\mathbf{J}_n]_{N+n+1,n} = \frac{K}{m_{n+1}}. \tag{18}$$

Substituting this expression, together with Eq. (14) and the eigenvectors of $\mathbf{G}$ and $\mathbf{G}^\dagger$, into Eq. (15) gives

$$\begin{aligned} J_n = \frac{2k_B K}{m_{n+1}} \sum_{k,l=1}^{2N} \Bigg[& \frac{\left(v^R_{N+n+1,l}\right)^* v^R_{n,k}}{\lambda_k + \lambda_l^*} \\ & \times \sum_{m=1}^{N} \gamma_m T_m \left(v^L_{N+m,k}\right)^* v^L_{N+m,l} \Bigg]. \end{aligned} \tag{19}$$

IV. HEAT CURRENT IN THE SMALL γ REGIME

The most convenient way to analyze the small γ dynamics of the 1D lattice is to perform a perturbation expansion of eigenvalues and eigenvectors of operator $\mathbf{G}$ with respect to γ. $\mathbf{G}$ is at most linear with respect to γ and can be represented as $\mathbf{G} = \mathbf{G}_0 + \gamma\mathbf{G}_1$, where $\mathbf{G}_{0,1}$

are independent of γ. The zeroth-order eigenvalues and eigenvectors of $\mathbf{G}$ are then the eigenvalues and eigenvectors of $\mathbf{G}_0$,

$$\mathbf{G}_0 = \begin{pmatrix} \mathbf{0} & -\mathbf{M}^{-1} \\ \mathbf{K} & \mathbf{0} \end{pmatrix}. \tag{20}$$

The solutions – normal modes of lattice vibrations with no friction – can be found in the standard way, first by scaling ("mass-weighting") by $\mathbf{S} = \mathrm{diag}(\mathbf{M}^{1/2}, \mathbf{M}^{-1/2})$,

$$\mathbf{S}\mathbf{G}_0\mathbf{S}^{-1} = \begin{pmatrix} \mathbf{0} & -\mathbf{I} \\ \mathbf{M}^{-\frac{1}{2}}\mathbf{K}\mathbf{M}^{-1/2} & \mathbf{0} \end{pmatrix} \tag{21}$$

and then diagonalizing the mass-weighted coupling $\mathbf{M}^{-1/2}\mathbf{K}\mathbf{M}^{-1/2}$ via an orthogonal transformation $\mathbf{T}$. The normal modes of the lattice are

$$x_n^k(t) = u_n^k e^{\pm i\omega_k t}, \tag{22}$$

where $u_n^k = \left[\mathbf{M}^{-1/2}\mathbf{T}\right]_{nk}$ are the real-valued polarization vectors of the normal modes and $n, k = 1, \ldots, N$ enumerate the lattice sites and modes, respectively.

The eigenvalues and *right* eigenvectors (hence denoted with R below) of $\mathbf{G}_0$ can be readily constructed from these and they come in pairs. The unnormalized "positive frequency" solutions are

$$\begin{aligned} \lambda_k^0 &= i\omega_k, \\ v_{n,k}^{0,R} &\propto u_n^k, \\ v_{N+n,k}^{0,R} &\propto -i\omega_k m_n u_n^k, \end{aligned} \tag{23}$$

for $k = 1, \ldots, N$ and $n = 1, \ldots, N$. The unnormalized "negative frequency" solutions are

$$\begin{aligned} \lambda_k^0 &= -i\omega_k, \\ v_{n,k}^{0,R} &\propto u_n^k, \\ v_{N+n,k}^{0,R} &\propto i\omega_k m_n u_n^k, \end{aligned} \tag{24}$$

for $k = N+1, \ldots, 2N$, $n = 1, \ldots, N$, and "extending" $\omega_k = \omega_{k-N}$ and $u_n^k = u_n^{k-N}$ for $k > N$. We have ordered the solution so that when the positive frequency solution takes on the label k, the negative frequency solution takes on the label $k+N$. The last two lines of each of these solutions reflect the simple relationship between momenta and the time derivative of coordinates, the first line in Eq. (6).

The left eigenvectors can be found in a similar way, essentially the position and momenta change roles including how they are scaled by mass. With the convention that $[\langle k_L|]_n = \left(v_{n,k}^L\right)^*$, the unnormalized "positive frequency" solutions are

$$\begin{aligned} \lambda_k^0 &= i\omega_k, \\ v_{n,k}^{0,L} &\propto i\omega_k m_n u_n^k, \\ v_{N+n,k}^{0,L} &\propto u_n^k, \end{aligned} \tag{25}$$

for $k = 1, \ldots, N$ and $n = 1, \ldots, N$. The unnormalized "negative frequency" solutions are

$$\begin{aligned} \lambda_k^0 &= -i\omega_k, \\ v_{n,k}^{0,L} &\propto -i\omega_k m_n u_n^k, \\ v_{N+n,k}^{0,L} &\propto u_n^k, \end{aligned} \tag{26}$$

for $k = N+1, \ldots, 2N$, $n = 1, \ldots, N$, and the same "extension" for $k > N$. The left and right eigenvectors clearly obey the right orthogonality relationship, but for each k have norm $\mp 2i\omega_k$ for "positive" and "negative" frequencies, respectively.

The first-order perturbative correction to the eigenvalues of $\mathbf{G}_0$ can be found in the usual manner, i.e.,

$$\lambda_k^1 = \gamma \langle k_L^0 | \mathbf{G}_1 | k_R^0 \rangle. \tag{27}$$

Using this expression, we can now expand the current. To do so, we will make use of Eq. (15). The matrix element $\langle k_L|\mathbf{F}|l_L\rangle$ is linear with respect to γ at small γ, i.e., putting in the normalized zeroth order states $\langle k_L^0|\mathbf{F}|l_L^0\rangle = \sum_n 2\gamma_n k_B T_n u_n^k u_n^l / \sqrt{4\omega_k\omega_l}$. Thus, we can focus on the quantity

$$\frac{\langle l_R|\mathbf{J}_n|k_R\rangle}{\lambda_k + \lambda_l^*} \tag{28}$$

and show that it is zeroth order with respect to γ. We separate the summation in Eq. (15) into the off-diagonal ($k \neq l$) and diagonal ($k = l$) contributions. Assuming no degeneracy, the former is nonzero and well-behaved when zeroth-order eigenvalues and eigenvectors are used since the denominator in Eq. (15) does not vanish at $k \neq l$. The off-diagonal contribution is thus proportional to γ at small γ.

The diagonal contribution has a vanishing denominator as γ approaches zero, i.e., λ_k^0 is pure imaginary which gives $\lambda_k + \lambda_k^* = 0 + \sum_n \gamma_n (u_n^k)^2 + \mathcal{O}(\gamma^2)$. Performing the whole sum, however, we can pair the "positive" and "negative" frequencies:

$$\sum_{k=1}^{N} \left(\langle k_R|\mathbf{J}_n|k_R\rangle + \langle (k+N)_R|\mathbf{J}_n|(k+N)_R\rangle \right) \frac{\langle k_L^0|\mathbf{F}|k_L^0\rangle}{\lambda_k + \lambda_k^*} \tag{29}$$

where the last factor is the same for both "positive" and "negative" frequencies. The term in parenthesis gives

$$\left(\frac{i m_{n+1} u_{n+1}^k u_n^k}{2} + \frac{-i m_{n+1} u_{n+1}^k u_n^k}{2} + \mathcal{O}(\gamma) \right) = 0 + \mathcal{O}(\gamma) \tag{30}$$

Thus, the sum over "positive" and "negative" frequencies gives a contribution that is of order γ. Therefore, the current for small γ is $J \propto \gamma$.

V. HEAT CURRENT IN THE LARGE γ REGIME

The current in the large γ regime can also be calculated perturbatively in powers of $1/\gamma$. We consider only single sites at each end connected to Langevin reservoirs, as any additional sites in the extended reservoir are decoupled from the lattice by higher orders in $1/\gamma$. Now consider the matrix $\gamma\mathbf{G}_1 + \mathbf{G}_0$, where $\mathbf{G}_0$ is the perturbation. The expansion is complicated by the fact that the "bare" matrix

$$\gamma\mathbf{G}_1 = \begin{pmatrix} \mathbf{0} & \mathbf{0} \\ \mathbf{0} & \mathbf{\Gamma M}^{-1} \end{pmatrix} \tag{31}$$

is highly degenerate, with $2N-2$ zero eigenvalues and 2 non-zero eigenvalues. The latter two are γ/m_1 and γ/m_N, which may have an (unimportant) degeneracy, and we can take two of the zeroth order right (left) eigenvectors to be $|N+1\rangle$ and $|2N\rangle$ ($\langle N+1|$ and $\langle 2N|$).

The degenerate space is spanned by the states $|n\rangle$ with $n = 1, \ldots, N$ and $|N+m\rangle$ with $m = 2, \ldots, (N-1)$. The degeneracy is lifted in the normal way: Let $\mathbf{P}_0$ project onto this subspace and diagonalize $\mathbf{P}_0\mathbf{G}_0\mathbf{P}_0$. This matrix has $2N-4$ eigenvectors with non-zero eigenvalues. The right eigenvectors with non-zero eigenvalues have the same form as Eqs. (23) and (24) except found from the lattice sites $2, \ldots, (N-1)$ only. The other two eigenvectors have a zero eigenvalue. Their degeneracy is not broken until the next order ($1/\gamma$), and requires diagonalizing

$$\mathcal{G} = \mathbf{P}_0\mathbf{G}_0\mathbf{P}_0 - \frac{1}{\gamma}\mathbf{P}_0\mathbf{G}_0\tilde{\mathbf{P}}_0\frac{1}{\mathbf{G}_1}\tilde{\mathbf{P}}_0\mathbf{G}_0\mathbf{P}_0, \tag{32}$$

with $\tilde{\mathbf{P}}_0 = (\mathbf{I} - \mathbf{P}_0)$. This matrix has a simple form

$$\begin{aligned}\mathcal{G} = &-\sum_{n\neq 1,N}\frac{1}{m_n}|n\rangle\langle N+n| + \sum_{n\neq 1,N;m} K_{nm}|N+n\rangle\langle m| \\ &+\frac{1}{\gamma}\sum_{n=1,N;m} K_{nm}|n\rangle\langle m|.\end{aligned} \tag{33}$$

Using this, we can search for the remaining two linearly independent and stable right eigenvectors with an eigenvalue of order $1/\gamma$. This results in a generalized eigenvalue problem for the zeroth order right eigenvectors, $\mathbf{K}|\lambda^0\rangle = \lambda\mathbf{B}|\lambda^0\rangle$ where $[\mathbf{B}]_{nm} = \delta_{nm}(\delta_{n1} + \delta_{nN})$. When this eigenvector is extended to the full degenerate space (padding it with zeros for all the momentum components), one has $\mathcal{G}|\lambda^0\rangle \approx \lambda/\gamma|\lambda^0\rangle$.

Starting with these zeroth order eigenvectors, then we can apply perturbation theory as usual. This results in three sets of eigenvectors, ($\mathcal{B}_1$) ones with eigenvalues that are $\mathcal{O}(\gamma)$ ($|N+1\rangle$ and $|2N\rangle$), ($\mathcal{B}_0$) ones that are $\mathcal{O}(1)$ (Eqs. (23) and (24) but in the internal lattice), and ($\mathcal{B}_{-1}$) ones that are $\mathcal{O}(1/\gamma)$ ($\mathbf{K}|\lambda^0\rangle = \lambda\mathbf{B}|\lambda^0\rangle$). We can also delineate these sets by the subspace on which the zeroth order eigenvectors live ($\mathcal{B}_1$ on ($|N+1\rangle$ and $|2N\rangle$; $\mathcal{B}_0$ on $|n\rangle$ with $n = 2, \ldots, (N-1)$ and $|N+m\rangle$ with $m = 2, \ldots, (N-1)$; $\mathcal{B}_{-1}$ on $|n\rangle$ with $n = 1, \ldots, N$). Contributions to the eigenvectors outside this subspace will be order $1/\gamma$. As with the small γ regime, we need to group the different contributions into diagonal and off-diagonal (and then further distinguish between off-diagonal contributions between these three groups). We will break down the contributions to Eq. (15) in terms of each of the factors $\langle l_R|\mathbf{J}|k_R\rangle$, $\langle k_L|\mathbf{F}|l_L\rangle$, and $(\lambda_k + \lambda_l^*)^{-1}$.

$\downarrow k \neq l \rightarrow$	$l \in \mathcal{B}_{-1}$	$l \in \mathcal{B}_0$	$l \in \mathcal{B}_1$
$k \in \mathcal{B}_{-1}$	$\frac{1}{\gamma}\cdot\frac{1}{\gamma}\cdot\gamma$	$1\cdot\frac{1}{\gamma}\cdot 1$	$\frac{1}{\gamma}\cdot 1\cdot\frac{1}{\gamma}$
$k \in \mathcal{B}_0$	$1\cdot\frac{1}{\gamma}\cdot 1$	$1\cdot\frac{1}{\gamma}\cdot 1$	$1\cdot 1\cdot\frac{1}{\gamma}$
$k \in \mathcal{B}_1$	$\frac{1}{\gamma}\cdot 1\cdot\frac{1}{\gamma}$	$1\cdot 1\cdot\frac{1}{\gamma}$	$\frac{1}{\gamma}\cdot 0\cdot\frac{1}{\gamma}$

TABLE I. Order of the different factors, $\langle l_R|\mathbf{J}|k_R\rangle\cdot\langle k_L|\mathbf{F}|l_L\rangle\cdot(\lambda_k+\lambda_l^*)^{-1}$, in the current contribution, Eq. 15, when $k \neq l$. Note that cross terms between $\mathcal{B}_1$ and $\mathcal{B}_1$ are identically zero given our choice of zeroth order eigenvectors.

We start with the diagonal contributions. For eigenvectors in $\mathcal{B}_1$, we get contributions to $\langle l_R|\mathbf{J}|k_R\rangle$; $\langle k_L|\mathbf{F}|l_L\rangle$; $(\lambda_k + \lambda_l^*)^{-1}$ of: at most $\mathcal{O}(1/\gamma)$ due to the zeroth order states living on $\{|N+1\rangle, |2N\rangle\}$; $\mathcal{O}(\gamma)$ as, e.g., $\langle N+1|\mathbf{F}|N+1\rangle = \mathcal{O}(\gamma)$; $\mathcal{O}(1/\gamma)$ because $\lambda_k \approx \gamma$. This gives an overall contribution at most of order $1/\gamma$.

For eigenvectors in $\mathcal{B}_0$, we get $\mathcal{O}(1)$ (this is the same calculation as Eq. (30), as the states are eigenstates of $\mathbf{G}_0$ on the internal lattice); $\mathcal{O}(1/\gamma)$ because although $\mathbf{F}$ is order γ, the contribution of $|N+1\rangle$ and $|2N\rangle$ to the eigenvector are order $1/\gamma$; $\mathcal{O}(\gamma)$ because the eigenvalue has a real part that is order $1/\gamma$ (the imaginary part is order 1 but this cancels in $\lambda_k + \lambda_l^*$). Thus, the total contribution from a eigenvector in $\mathcal{B}_0$ is order 1. However, just like in Eq. (30) for the small γ regime, this contribution always has a paired contribution from the negative and positive frequency mode, which cancels this order 1 contribution. This gives an overall contribution at most of order $1/\gamma$.

For eigenvectors in $\mathcal{B}_{-1}$, we get $\mathcal{O}(1/\gamma)$ due to the zeroth order eigenvector living only on the position component of the vector; $\mathcal{O}(1/\gamma)$ because although $\mathbf{F}$ is order γ, the contribution of $|N+1\rangle$ and $|2N\rangle$ to the eigenvector are order $1/\gamma$; $\mathcal{O}(\gamma)$ because the eigenvalue has a real part of order $1/\gamma$. This gives an overall contribution at most of order $1/\gamma$.

For the off-diagonal terms, we give the contributions to each of the three factors for all the different possibilities in Table I. The highest order contributions from the off

diagonal are order $1/\gamma$. Thus, the sum over all contributions gives zero for the zeroth order term and the leading term is order $1/\gamma$.

We note that for both the small γ and large γ regimes, these well-defined perturbation expansions demonstrate that the the zeroth order terms are zero, a fact which is obvious for the small γ regime (i.e., there would be no driving force for the thermal current) but not the large γ regime. Moreover, due to the presence of the different temperature reservoirs at each end, the first order expressions are non-zero always unless the lattice has a broken link. Coupled with the results of the anharmonic lattice, the perturbative expressions give evidence that the presence of these regimes are universal except in pathological cases.